Clim Dyn
DOI 10.1007/s00382-012-1604-9

# Evaluation of twentieth-century Atlantic Warm Pool simulations in historical CMIP5 runs

**Michael E. Kozar · Vasubandhu Misra**

Received: 13 July 2012 / Accepted: 15 November 2012


**Abstract** State-of-the-art coupled global climate models are evaluated for their simulation of the Atlantic Warm Pool (AWP). Historical runs from 17 coupled climate models included in the Fifth Phase of the Coupled Model Intercomparison Project (CMIP5) serve as the basis for this model evaluation study. The model simulations are directly compared to observations and reanalysis data to evaluate the climatological features and variability of the AWP within each individual model. Results reveal that a select number of models—namely the GISS-E2-R, CSIRO-Mk3.6, and MPI-ESM-LR—are successful at resolving an appropriately sized AWP with some reasonable climatological features. However, these three models exhibit an erroneously broad seasonal peak of the AWP, and its variability is significantly underestimated. Furthermore, all of the CMIP5 models exhibit a significant cold bias across the tropical Atlantic basin, which hinders their ability to accurately resolve the AWP.

**Keywords** Atlantic Warm Pool · CMIP5 · Tropical North Atlantic Climate

## 1 Introduction

The Atlantic Warm Pool (AWP) is a component of the Western Hemisphere Warm Pool (Wang and Enfield 2001, 2003) in the Intra-Americas Seas (IAS) region of the Tropical North Atlantic (TNA) basin. Much like warm pools in other regions of the globe, the AWP influences both the local and the remote climate. However, unlike other warm pool systems (i.e., the Western Pacific Warm Pool) the AWP is not defined in each season of the year. The AWP, which exists entirely north of the equator, is not defined during the cooler boreal winter months, as the sea surface temperatures (SSTs) throughout the IAS remain well below the threshold of 28.5 °C that is used to define the bounds of the AWP. The AWP typically emerges during the late spring months as the Gulf of Mexico and the Caribbean Sea warm. The AWP then evolves into a well-developed region of warmer waters well in excess of 28.5 °C during the boreal summer and early fall (Wang et al. 2006). This seasonal variation is thought to exist because of differential clear-sky radiation flux (Lee et al. 2007), coastal upwelling, the influence of the North Atlantic Subtropical High (NASH), Caribbean low-level jet (CLLJ; Wang and Lee 2007), and local meridional circulations, as well as rainfall patterns over South America and the subsequent discharge into the region from the Amazon and Orinoco Rivers (Misra and DiNapoli 2012; Vizy and Cook 2010).

In addition to seasonal variability, the AWP also exhibits interannual and longer scale variability with respect to its areal extent and its intensity (e.g., Wang and Enfield 2001; Wang et al. 2008). In some years (e.g., 1937, 2005), the summertime AWP may become anomalously large, stretching from the Gulf of Mexico well into the central Atlantic, while in other years (e.g., 1913, 1984), a smaller summertime AWP may be confined to only a portion of the Gulf of Mexico. Such variability in the size of the AWP is thought to be connected to modes of variability in the global climate system such as the Atlantic Multidecadal Oscillation (AMO), the North Atlantic Oscillation (NAO), or the El Niño-Southern Oscillation (ENSO) (e.g., Covey and Hastenrath 1978; Enfield and

M. E. Kozar (✉) · V. Misra
Department of Earth, Ocean and Atmospheric Science, Center for Ocean–Atmospheric Prediction Studies (COAPS), Florida State University, 2035 E. Paul Dirac Dr., 200 RM Johnson Bldg., Tallahassee, FL 32306-2840, USA
e-mail: mkozar@coaps.fsu.edu

Published online: 25 December 2012

Mayer 1997; Czaja et al. 2002; Wang and Enfield 2003; Enfield et al. 2006; Wang et al. 2008; Liu et al. 2012).

Furthermore, variability of the AWP is thought to have effects on the surrounding TNA climate. Anomalously large AWPs are thought to weaken the dominant NASH (Wang et al. 2007). Therefore, wind patterns throughout the Atlantic basin, including but not limited to the CLLJ and the Great Plains low-level jet (GPLLJ), are also influenced by the AWP (Wang et al. 2007). Through its influence over regional wind and SST patterns, the AWP is also well known to influence the variability of smaller scale features, such as atmospheric convection and North Atlantic tropical cyclones (e.g., Wang et al. 2006, 2011; Wang and Lee 2007). More specifically the AWP, by its definition, exceeds the convective SST threshold ($\sim$26–27 °C) needed to support large-scale organized convection that elicits a Gill-type atmosphere response (Wang et al. 2007). As such, large-scale convection will not occur in the absence of a large area of warm sea surface temperatures such as the AWP (e.g., Hoyos and Webster 2011). Therefore, examining the fidelity of a climate model in simulating the AWP is important to understanding the TNA climate system.

Despite advancements in climate modeling in the past decade, realistic simulations of the TNA climate have remained elusive (e.g., Davey et al. 2002; Chang et al. 2007; Richter and Xie 2008; Grodsky et al. 2012). The coupled ocean-atmospheric general circulation models (GCMs) used in the fourth assessment (AR4) of the Intergovernmental Panel on Climate Change (IPCC) contained multiple biases in their simulations of the TNA (e.g., Richter and Xie 2008; Liu et al. 2012). Some of the biases, specifically the tropical wind biases in CCSM3, are thought to be a result of erroneous simulations of Amazon rainfall and its teleconnection to the TNA (Chang et al. 2008). Considering the importance of the AWP to TNA variability, it is not surprising that many of the models included in IPCC's AR4 failed to reproduce the observed AWP; some even placed an erroneous cold pool in the IAS (Misra et al. 2009). On the eastern side of the TNA, the majority of these same models also failed to reproduce the eastern equatorial Atlantic cold tongue because of a warm bias in the tropical South Atlantic extending to the Angolan and Namibian coastlines (Liu et al. 2012). The failure to reproduce the cold tongue is a common performance flaw in coupled GCMs, resulting in the reversal of the equatorial Atlantic climatological SST gradient (Richter and Xie 2008; Richter et al. 2012).

Recently, a new set of integrations from the state-of-the-art collection of coupled models has been produced in support of the Fifth Phase of the Coupled Model Intercomparison Project (CMIP5; e.g., Taylor et al. 2012) and the IPCC's upcoming assessment report (AR5). Understanding how these CMIP5 models have improved in their simulations of the AWP region compared to their previous iterations will have implications on the potential realism of the tropical-subtropical western hemisphere climate system. Therefore, the goal of this study is to assess how well the historical runs of the CMIP5 models simulate the AWP's climatology and its different modes of variability with respect to twentieth-century observations and reanalysis.

## 2 Data and methods

### 2.1 CMIP5 models

The broad selection of CMIP5 models used in this study comprises 17 coupled climate models, developed by 14 institutions across 10 countries (Table 1). The focus of this study is to evaluate these model integrations with respect to observations and reanalysis. Therefore, the core of this analysis relies on historical runs from each model forced by observed twentieth-century emissions. The length of each historical simulation varies slightly from model to model, but in general each model runs from the mid-to-late nineteenth century to the first few years of the twenty-first century. Only one (r1i1p1) monthly mean ensemble member from each of the models is analyzed in this study for the sake of simplicity.

The ocean surface temperature fields in each model (designated by the CMIP5 as 'tos') are examined first to properly assess how each model reproduces the AWP. From the SST fields, we create a monthly AWP area index (AWPAI), measured by the enclosed area of the 28.5 °C contour in the northwest Atlantic (0°N–45°N; 100°W–40°W). Such an index is useful in determining the summertime size and variability of the AWP, as well as its seasonal cycle in each simulation. It is possible that the 28.5 °C SST contour is not the best method for defining the AWP within the model simulations if they have a basin-wide cold bias. However, using a lower temperature threshold becomes problematic because the CMIP5 models, like the CMIP3 models before them (Richter and Xie 2008), fail at producing the observed Atlantic cold tongue in the equatorial Eastern Atlantic. Therefore, lowering the temperature threshold for the AWP below 28.5 °C would likely include warm waters in the equatorial Atlantic, which are not part of the traditionally defined AWP in observations.

To supplement this analysis, a number of other oceanic and atmospheric fields are also examined including, but not limited to, ocean potential temperature ('thetao'), atmospheric temperature ('ta'), sea level pressure ('psl'), meridional winds ('va'), and zonal winds ('ua'). All of these fields within the CMIP5 models, including the SST

**Table 1** A list of CMIP5 models and their respective modeling institutions which are analyzed in this study

| Institution | Model |
|---|---|
| Beijing Climate Center, China Meteorological Administration | BCC-CSM1-1 |
| Canadian Centre for Climate Modelling and Analysis | CanESM2 |
| Centre National de Recherches Meteorologiques/ Centre Europeen de Recherche et Formation Avancees en Calcul Scientifique | CNRM-CM5 |
| Commonwealth Scientific and Industrial Research Organisation in collaboration with the Queensland Climate Change Centre of Excellence | CSIRO-Mk3.6 |
| Institute for Numerical Mathematics | INM-CM4 |
| Institut Pierre-Simon Laplace | IPSL-CM5A-LR |
| Atmosphere and Ocean Research Institute (The University of Tokyo), National Institute for Environmental Studies, and Japan Agency for Marine–Earth Science and Technology | MIROC5 |
| Met Office Hadley Centre | HadGEM2-ES |
| Max Planck Institute for Meteorology | MPI-ESM-LR |
| Meteorological Research Institute | MRI-CGCM3 |
| NASA Goddard Institute for Space Studies | GISS-E2-H |
| | GISS-E2-R |
| NOAA Geophysical Fluid Dynamics Laboratory | GFDL-CM3 |
| | GFDL-ESM2G |
| | GFDL-ESM2M |
| National Center for Atmospheric Research | CCSM4 |
| Norwegian Climate Centre | NorESM1-M |

data mentioned above, have been linearly detrended. Analysis of this expansive set of model data will help to determine whether the models are capturing the observed physical processes that control the AWP.

### 2.2 Observations and reanalysis

The third version of the Extended Reconstructed Sea Surface Temperature analysis (ERSSTv3; Smith et al. 2008) serves as the observational baseline for analysis of the SST fields in the models. ERSSTv3 is generated using in situ SST data and statistical methods to reconstruct global SSTs from sparse data at a spatial resolution of 2° longitude by 2° latitude. The ERSST v3 data are available as monthly means from 1854 to present; however, only the years 1909–2005 are used in the present analysis to avoid the period of sparse data in the early part of the record. Therefore, to ensure consistency, all analysis in the upcoming sections will focus on this 1909–2005 interval, which is the longest period of time in which observations and model data for this study overlap.

The CMIP5 results are validated with the National Center for Environmental Prediction's (NCEP) and the Department of Energy's (DOE) Reanalysis-2 project (R-2; Kanamitsu et al. 2002). For the purposes of this study, 1979–2011 monthly means from R-2 of sea level pressure and 925 hPa u- and v-winds are used for a direct comparison to the monthly means of the historical CMIP5 runs.

The European Centre for Medium-Range Weather Forecasts' (ECMWF) ERA-40 reanalysis dataset (Uppala et al. 2005) was also considered, but ultimately left out of the present analysis. Both the ERA-40 and the R-2 datasets have very similar 925 hPa wind and mean sea level pressure fields over the North Atlantic, which suggests that using ERA-40 as a second reanalysis dataset, in addition to R-2, would not add much value to the results. A recent intercomparison study of AWP variability in atmospheric reanalysis by Misra et al. (2012) confirms this by noting that atmospheric response to AWP in R-2 was comparable to other modern reanalyses (e.g., Saha et al. 2010; Rienecker et al. 2011).

## 3 Results

### 3.1 Overview of AWP climatology in 17 CIMP5 models

The average size of the AWP (defined by the 28.5 °C SST contour) during its peak season of August–September–October (ASO) from 1909 to 2005 is just over 2.8 million km$^2$ in the ERSSTv3 observations. Statistics from the observed and model-derived ASO averaged AWPAI are shown in Table 2. Only the CSIRO-Mk3.6 and the GISS-E2-R produce an average ASO AWP comparable in size to the observations. The GISS-E2-R is noteworthy for being the only model to produce an AWP larger than the observations on average. Conversely, this means that most of the models underestimate the average size of the summertime AWP. In 15 of the 17 model simulations (~88 %), the ASO averaged AWP has an areal extent less than half of the observed 2.8 million km$^2$.

Similarly, a majority of the models underestimate the interannual variations of the AWPAI (Table 2). The observed AWP can grow large some years, extending westward into the central Atlantic whereas in other years, the AWP can be essentially undefined all year long. For example in 1913, the observed AWP covered less than 0.05 million km$^2$, whereas in 2005, the AWP covered more than 6.6 million km$^2$. Only the GISS-E2-R, MPI-ESM-LR, GISS-E2-H, CSIRO-Mk3.6, and HadGEM2-ES can produce AWPs larger than 3 million km$^2$. However, with the exception of the GISS-E2-H, those five models tend to have a well-defined ASO averaged AWP of at least

100,000 km$^2$ each year from 1909 to 2005, meaning they are unable to reproduce the occasionally observed extremely small AWPs. The other 12 models fail to produce the larger AWPs. For example, the largest single ASO AWP in each of these 12 models is still smaller than the mean observed ASO AWP. Such an under-representation of the AWP in more than half the models ultimately suggests that many of the models have a cold bias across the Atlantic Basin.

Past works (e.g., Clement et al. 2005) found that the global tropics have a skewed SST distribution, in terms of percent of total area. ASO observations show that the North Atlantic basin region (0°N–45°N; 100°W–40°W) also has a skewed SST distribution (Table 3). More than 70 % of the northwest Atlantic Ocean has SSTs between 26 and 29 °C. Only 16.6 % of the northwest Atlantic, by area, has SSTs between 20 and 26 °C, and only about 4 % of the basin has SSTs warmer than 29 °C, with the area covered by SSTs greater than 30 °C being negligible.

The majority of the models fail to reproduce the observed summertime Atlantic SST distribution correctly (Table 3). Some models (e.g., MIROC5, CSIRO-Mk3.6, IPSL-CM5-A) have a more normal looking distribution, without the skewness that is observed in the ERSSTv3 distribution. Most of the models, however, are hindered by a significant cold SST bias. As a result, all of the models over-represent the 24–25 and 25–26 °C bins, and all models except the GISS-E2-R under-represent the 28–29 °C bin. Since the AWP is defined by SSTs greater than 28.5 °C, the 28–29 °C and the 29–30 °C bins are the most relevant to this study. Table 2 indicates that the CSIRO-Mk3.6, GISS-E2-R, and the MPI-ESM-LR have the largest AWPs. Unsurprisingly, a significant portion (19–31 %) of the simulated TNA ocean in these models exhibits SSTs >28 °C (compared to 30.4 % in observations). The CSIRO-Mk3.6 is different from the other two models as it does not have a skewed distribution, and it overestimates the area covered by SSTs >30 °C as a result.

**Table 2** Statistics, in $10^6$ km$^2$, from the 1909–2005 model-derived and observed AWP areal index time series plotted in Fig. 1

| | Mean | Median | SD | Maximum | Minimum |
|---|---|---|---|---|---|
| *Observations* | | | | | |
| ERSST v3 | 2.817 | 2.593 | 1.350 | 6.670 | 0.046 |
| *Models* | | | | | |
| BCC-CSM1-1 | 0.127 | 0.074 | 0.141 | 0.527 | 0.000 |
| CanESM2 | 0.338 | 0.250 | 0.392 | 2.250 | 0.000 |
| CCSM4 | 0.464 | 0.297 | 0.479 | 2.620 | 0.000 |
| CNRM-CM5 | 0.303 | 0.248 | 0.199 | 1.087 | 0.089 |
| CSIRO-Mk3.6 | 2.337 | 2.345 | 0.696 | 3.772 | 0.716 |
| GFDL-CM3 | 0.297 | 0.192 | 0.329 | 1.574 | 0.000 |
| GFDL-ESM2G | 0.251 | 0.179 | 0.197 | 0.914 | 0.023 |
| GFDL-ESM2M | 0.279 | 0.232 | 0.191 | 1.122 | 0.037 |
| GISS-E2-H | 0.637 | 0.307 | 0.728 | 3.921 | 0.000 |
| GISS-E2-R | 2.984 | 2.755 | 0.995 | 6.013 | 0.963 |
| HadGEM2-ES | 0.834 | 0.656 | 0.554 | 3.558 | 0.229 |
| INM-CM4 | 0.001 | 0.000 | 0.003 | 0.017 | 0.000 |
| IPSL-CM5A-LR | 0.028 | 0.000 | 0.047 | 0.174 | 0.000 |
| MIROC5 | 0.151 | 0.105 | 0.149 | 0.939 | 0.022 |
| MPI-ESM-LR | 1.360 | 0.991 | 1.081 | 4.125 | 0.118 |
| MRI-CGCM3 | 0.249 | 0.243 | 0.164 | 1.026 | 0.000 |
| NorESM1-M | 0.000 | 0.000 | 0.001 | 0.007 | 0.000 |

As previously mentioned, the AWP has a distinct seasonal cycle. Wang et al. (2006) noted that the AWP should be well defined only in the summer months, with a relatively sudden onset and dissipation. This is seen in the ERSSTv3 observations (Table 4), as the area of the AWP ramps up in July, reaches its peak in September, and rapidly diminishes in November. As a result of the cold biases in many of the CMIP5 models, the majority of models underestimate the size of the climatologically averaged AWP during all of the summer and fall months, and some models (INM-CM4; NorESM1-M) have essentially no traditionally defined AWP. The erroneous peak season AWP magnitudes are not the only glaring issue in the models representation of the AWP's seasonal cycle. In 10 of the 17 models ($\sim$59 % of the CMIP5 models), the AWP reaches its peak size in August, which is 1 month too early when compared to observations. Second, most of the models fail to reproduce the changes in the AWP's size during its abrupt onset in the early summer and its dissipation in the late autumn. Many of the colder models (BCC-CSM1-1, CCSM4, CanESM2, GFDL-CM3, INM-CM4, IPSL-CM5A-LR, NorESM1-M) weaken their modest AWPs much too quickly to the extent that by October, less than 20 % of the AWP's area remains with respect to its peak monthly size (compared to 41 % in the observations). The models less hindered by a cold bias, however, have an entirely different problem in that they fail to exhibit the sharp changes in the AWP's seasonal cycle. Four models—CSIRO-Mk3.6, GISS-E2-R, GISS-E2-H and HadGEM2-ES—have well-defined AWPs of over 200,000 km$^2$ into November (compared to 70,000 km$^2$ in the observations). The development of the AWP is much too gradual in these models in comparison to the sudden onset in the observations. The HadGEM2-ES in particular overestimates the average size of the warm pool during the spring and winter months, when the AWP is expected to be undefined.

### 3.2 AWP biases and errors in selected models

A more detailed analysis of a subsample of models (5 of the 17), featuring models that exhibit the most reasonable

**Table 3** Frequency distribution of 1909–2005 ASO averaged SSTs across the Atlantic Basin in one-degree bins

| Bin | ERSST v3 | BCC-CSM1-1 | CanESM2 | CCSM4 | CNRM-CM5 | CSIRO-Mk3.6 | GFDL-CM3 | GFDL-ESM2G | GFDL-ESM2M |
|---|---|---|---|---|---|---|---|---|---|
| 20-21 °C | 1.4% | 1.3% | 1.1% | 0.6% | 1.0% | 1.4% | 1.4% | 0.9% | 1.1% |
| 21-22 °C | 1.1% | 1.8% | 1.3% | 1.2% | 1.3% | 1.8% | 2.2% | 1.3% | 1.4% |
| 22-23 °C | 1.3% | 2.1% | 1.9% | 2.0% | 1.8% | 3.1% | 3.0% | 2.1% | 2.1% |
| 23-24 °C | 2.1% | 2.9% | 4.1% | 2.9% | 3.2% | 6.8% | 4.5% | 5.2% | 4.4% |
| 24-25 °C | 3.3% | 6.5% | 10.6% | 4.7% | 7.4% | 11.5% | 8.1% | 10.1% | 10.3% |
| 25-26 °C | 7.5% | 18.5% | 17.6% | 14.9% | 16.5% | 16.4% | 15.2% | 15.5% | 17.4% |
| 26-27 °C | 15.3% | 37.1% | 23.4% | 26.6% | 27.1% | 17.3% | 23.7% | 26.5% | 27.9% |
| 27-28 °C | 29.4% | 20.6% | 27.4% | 35.2% | 26.4% | 16.7% | 29.3% | 27.4% | 23.5% |
| 28-29 °C | 26.3% | 2.9% | 7.6% | 10.7% | 6.4% | 12.9% | 6.3% | 4.5% | 4.2% |
| 29-30 °C | 4.1% | 0.1% | 0.2% | 0.3% | 0.4% | 5.3% | 0.1% | 0.3% | 0.4% |
| >30°C | 0.0% | 0.0% | 0.0% | 0.0% | 0.0% | 1.1% | 0.0% | 0.0% | 0.0% |
| Bin | GISS-E2-H | GISS-E2-R | HadGEM 2-ES | INM-CM4 | IPSL-CM5A-LR | MIROC5 | MPI-ESM-LR | MRI-CGCM3 | NorESM1-M |
| 20-21 °C | 2.1% | 1.6% | 0.6% | 1.5% | 1.6% | 1.2% | 1.0% | 1.9% | 0.0% |
| 21-22 °C | 2.0% | 2.6% | 0.8% | 2.2% | 2.3% | 1.8% | 1.4% | 2.3% | 0.0% |
| 22-23 °C | 2.9% | 3.2% | 1.9% | 3.3% | 4.9% | 3.9% | 2.1% | 3.1% | 0.5% |
| 23-24 °C | 4.9% | 4.4% | 4.5% | 5.0% | 13.1% | 10.4% | 4.9% | 4.8% | 9.8% |
| 24-25 °C | 7.3% | 6.3% | 10.8% | 7.9% | 20.3% | 16.9% | 9.7% | 9.8% | 24.5% |
| 25-26 °C | 10.3% | 8.2% | 16.9% | 15.1% | 23.0% | 22.0% | 12.9% | 16.1% | 39.9% |
| 26-27 °C | 15.4% | 12.4% | 27.4% | 35.4% | 16.6% | 22.4% | 16.9% | 25.6% | 22.0% |
| 27-28 °C | 30.3% | 24.5% | 22.5% | 25.1% | 7.9% | 12.8% | 24.8% | 22.9% | 3.4% |
| 28-29 °C | 19.0% | 27.6% | 9.1% | 0.6% | 0.9% | 2.3% | 17.2% | 4.3% | 0.0% |
| 29-30 °C | 0.1% | 3.5% | 1.4% | 0.0% | 0.0% | 0.2% | 1.8% | 0.2% | 0.0% |
| >30°C | 0.0% | 0.0% | 0.3% | 0.0% | 0.0% | 0.1% | 0.0% | 0.0% | 0.0% |

Each value is shown in percent area of the total domain (0°N–45°N and 40°W–100°W), and is accompanied by a bar graph. The bins that contribute to the AWP (SST > 28.5°) are shown in red

AWP climatology, is presented in this subsection. The mean ASO SST fields from the observations and each of the five models are shown in Fig. 1. The first two models included in this discussion, GISS-E2-R and CSIRO-Mk3.6, have the most realistically sized climatological AWP, but they have two very different SST distributions in the tropical North Atlantic. Next, the MRI-ESM-LR is considered for its somewhat reasonable AWP climatology and seasonal cycle. The HadGEM2-ES is included in this section as it (erroneously) has a detectable AWP in all 12 months of the year on average. Lastly, the widely used CCSM4 is included in this analysis to examine why some models do not have an appropriately sized AWP.

The observed AWP emerges in the western part of the Gulf of Mexico and the Caribbean Sea and spreads eastward and to a lesser degree northward. From Fig. 1, it appears that the GISS-E2-R is the most realistic in terms of not only size but also position of the AWP. The large AWP in the CSIRO-Mk3.6, on the other hand, is located in the central Gulf of Mexico and the Caribbean Sea. The other three models (MRI-ESM-LR, HadGEM2-ES, and CCSM4) have smaller AWPs, but the 28.5 °C contour, when present, tends to be located in close proximity to land, whether it be the Gulf Coast, Central America, or the Caribbean Islands.

The differences between the SST fields in each of the five models and the observations are shown in Fig. 2.

**Table 4** Average monthly AWP areas (in $10^6$ km$^2$) from 1909 to 2005 based on various CMIP5 models and ERSSTv3 observations

Seasonal Cycle of AWP Area

| Months | Jan | Feb | Mar | Apr | May | Jun | Jul | Aug | Sep | Oct | Nov | Dec |
|---|---|---|---|---|---|---|---|---|---|---|---|---|
| ERSST v3 | 0.0010 | 0.0015 | 0.0020 | 0.0091 | 0.0486 | 0.3983 | 2.4866 | 3.7066 | 3.9859 | 1.6280 | 0.0706 | 0.0010 |
| BCC-CSM1-1 | 0.0000 | 0.0000 | 0.0000 | 0.0003 | 0.0006 | 0.0141 | 0.2934 | 0.6754 | 0.3805 | 0.0181 | 0.0000 | 0.0000 |
| CanESM2 | 0.0000 | 0.0000 | 0.0028 | 0.0085 | 0.0025 | 0.0265 | 0.2942 | 0.8290 | 0.7793 | 0.1535 | 0.0128 | 0.0000 |
| CCSM4 | 0.0000 | 0.0002 | 0.0024 | 0.0167 | 0.0204 | 0.0402 | 0.5120 | 1.3070 | 1.1203 | 0.1214 | 0.0019 | 0.0000 |
| CNRM-CM5 | 0.0004 | 0.0010 | 0.0031 | 0.0082 | 0.0227 | 0.0724 | 0.2707 | 0.7918 | 0.8510 | 0.2817 | 0.0250 | 0.0056 |
| CSIRO-Mk3.6 | 0.0000 | 0.0000 | 0.0000 | 0.0000 | 0.0437 | 0.4341 | 2.0641 | 2.9905 | 3.0941 | 1.4189 | 0.2617 | 0.0000 |
| GFDL-CM3 | 0.0001 | 0.0000 | 0.0004 | 0.0020 | 0.0025 | 0.0559 | 0.5422 | 1.1756 | 0.7579 | 0.1113 | 0.0033 | 0.0002 |
| GFDL-ESM2G | 0.0000 | 0.0000 | 0.0001 | 0.0009 | 0.0002 | 0.0084 | 0.1824 | 0.8142 | 0.8066 | 0.2210 | 0.0110 | 0.0001 |
| GFDL-ESM2M | 0.0000 | 0.0001 | 0.0003 | 0.0017 | 0.0049 | 0.0135 | 0.1406 | 0.6971 | 0.6439 | 0.2587 | 0.0203 | 0.0003 |
| GISS-E2-H | 0.0013 | 0.0038 | 0.0172 | 0.0917 | 0.1877 | 0.2572 | 0.3098 | 0.7030 | 1.0184 | 0.9023 | 0.2383 | 0.0089 |
| GISS-E2-R | 0.0031 | 0.0031 | 0.0176 | 0.1640 | 0.4012 | 0.6770 | 1.7286 | 3.5522 | 3.8256 | 2.8540 | 1.0380 | 0.0894 |
| HadGEM2-ES | 0.0516 | 0.0439 | 0.0586 | 0.1021 | 0.2070 | 0.3251 | 0.5714 | 1.3660 | 1.4805 | 0.5714 | 0.2056 | 0.0954 |
| INM-CM4 | 0.0061 | 0.0008 | 0.0001 | 0.0053 | 0.0192 | 0.0030 | 0.0059 | 0.0581 | 0.0212 | 0.0001 | 0.0025 | 0.0098 |
| IPSL-CM5A-LR | 0.0000 | 0.0000 | 0.0000 | 0.0001 | 0.0029 | 0.0250 | 0.0715 | 0.2065 | 0.0725 | 0.0063 | 0.0000 | 0.0000 |
| MIROC5 | 0.0000 | 0.0000 | 0.0004 | 0.0229 | 0.0435 | 0.0929 | 0.1080 | 0.2307 | 0.2562 | 0.1224 | 0.0200 | 0.0012 |
| MPI-ESM-LR | 0.0000 | 0.0000 | 0.0000 | 0.0009 | 0.0020 | 0.0752 | 0.7075 | 2.0492 | 2.4500 | 1.0084 | 0.1371 | 0.0107 |
| MRI-CGCM3 | 0.0000 | 0.0000 | 0.0000 | 0.0000 | 0.0024 | 0.0230 | 0.1204 | 0.3863 | 0.3844 | 0.1760 | 0.0050 | 0.0000 |
| NorESM1-M | 0.0000 | 0.0000 | 0.0000 | 0.0000 | 0.0000 | 0.0000 | 0.0032 | 0.0261 | 0.0209 | 0.0000 | 0.0000 | 0.0000 |

| 0.00 | 0.05 | 0.10 | 0.15 | 0.20 | 0.30 | 0.40 | 0.60 | 0.80 | 1.00 | 1.25 | 1.50 | 1.75 | 2.00 | 2.50 | 3.00 | 3.50 | 4.00 |
|---|---|---|---|---|---|---|---|---|---|---|---|---|---|---|---|---|---|

AREA OF 28.5°C MONTHLY AVERAGED ISOTHERM ($10^6$km$^2$)

Each cell in the table is color coded (cool colors indicate a small AWP; warm colors indicate a large AWP) in order to show the average seasonal evolution of the AWP's areal extent

Somewhat surprisingly, the GISS-E2-R has a cold bias across much of the North Atlantic and the Gulf of Mexico. However, the GISS-E2-R does have a weak warm bias over the Caribbean, where most of its large AWP is located. The CCSM4, MPI-ESM-LR, and HadGEM2-ES all have a predominant cold bias, as expected by their cold TNA SST distribution (Table 3). Ultimately, these three models have a cold bias of up to 2 °C across much of the IAS region, thus limiting the size of the AWP region. The CSIRO-Mk3.6 is interesting as it has a significant cold bias across most of the basin, yet it also has a sizable AWP. The reasonably sized AWP in the CSIRO-Mk3.6 is consistent with the small regional warm bias around the Caribbean Islands, which is already one of the warmest parts of the observed TNA. As shown in Table 3, the biases in the CSIRO-Mk3.6 ultimately lead to a more normal SST distribution. In addition, as alluded to earlier, the GISS-E2-R, CCSM4, MPI-ESM-LR, and Had-GEM2-ES also exhibit signs of a warm bias in the eastern Atlantic where the Atlantic cold tongue is expected to be, thus affecting the SST distribution and the SST gradient across the equatorial Atlantic. With exception to the CSIRO-Mk3.6, this tropical eastern Atlantic Warm bias extends southeast to the Southwest African coastline. Such an expansive warm bias indicates that the issues within the models are more complex than a simple westerly wind bias in the equatorial Atlantic.

As previously mentioned, the AWP is connected to the North Atlantic Subtropical High, whereas a large AWP is

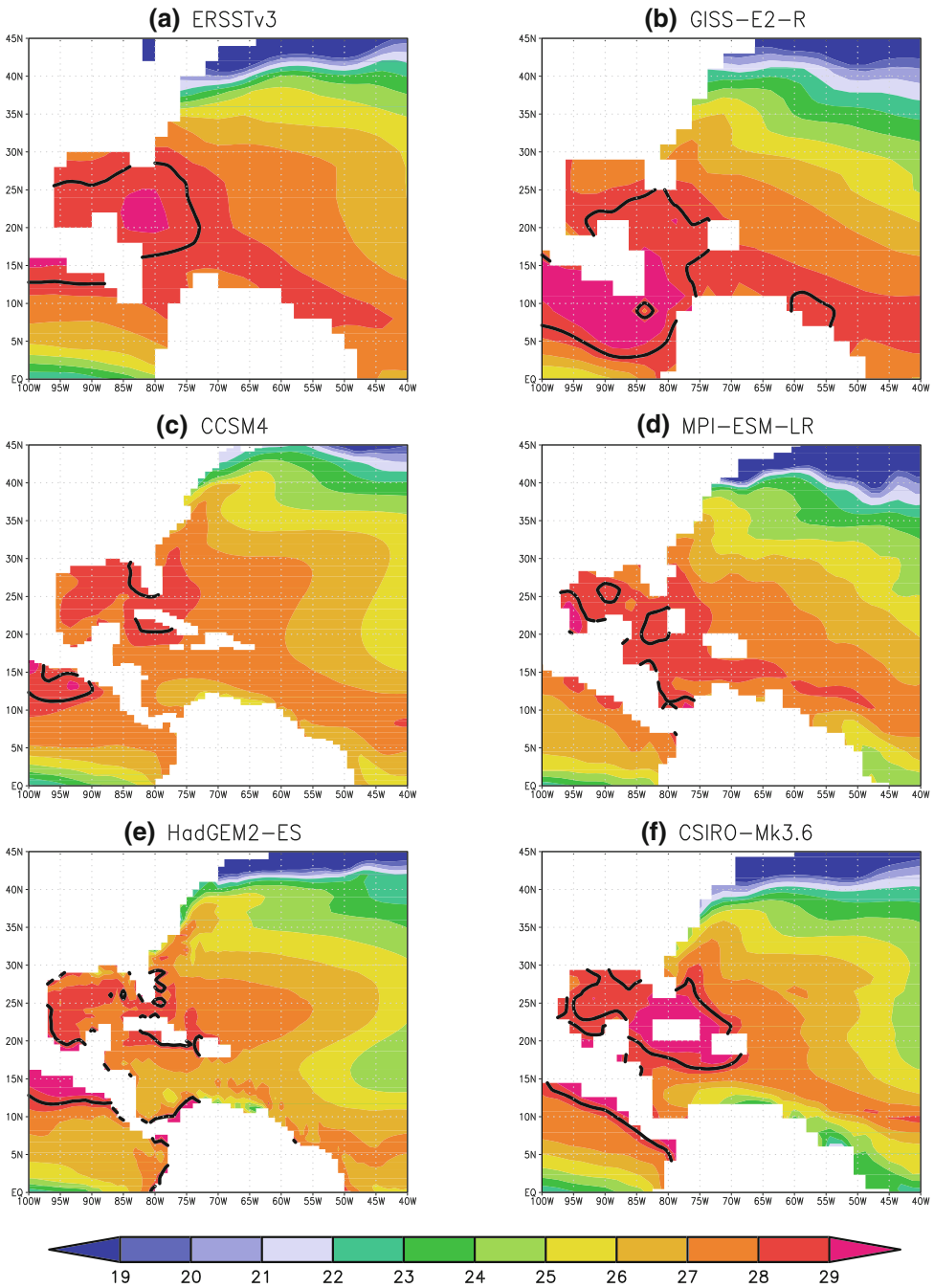


**Fig. 1** Climatological 1909–2005 ASO Average SST (°C) in the Atlantic Basin from (**a**) detrended ERSST v3 observations and (**b–e**) various detrended CMIP5 models. The mean 28.5 °C isotherm (*heavy black line*) is placed over the *shaded SSTs* to highlight the size and location of the AWP in each individual model

associated with a weakened NASH (Wang 2007). Figure 3 shows mean ASO sea level pressure across the Atlantic basin in the NCEP-DOE R-2, as well as deviations from the reanalysis data for each model. Here, the HadGEM2-ES seems to have the most reasonable pressure field of the five models when compared to the reanalysis data (Fig. 3e). The NASH, however, does appear to be farther south in the HadGEM2-ES compared to the reanalysis data, as evident by the higher pressures in the Caribbean and the lower pressures in the North Atlantic.

The CSIRO-Mk3.6 has lower sea level pressure in the western Atlantic with respect to the NCEP-DOE R-2. The low pressure bias leads to a weaker NASH, which is consistent with a larger AWP. However, the CSIRO-Mk3.6 has an apparent low pressure bias over land (of 4 hPa or more over areas like South America), which in turn may be responsible for the lower pressure in the AWP region. Likewise, the MPI-ESM-LR has a weaker than expected NASH that has been shifted to the northeast (Fig. 3d). Unlike the CSIRO-Mk3.6 and MPI-ESM-LR, the GISS-

E2-R has a more extreme low pressure bias of 2 hPa or more that, curiously, extends throughout the entire TNA (Fig. 3b). The significantly weaker NASH is consistent with the larger AWP that exists in the GISS-E2-R.

In contrast, the CCSM4 has a high pressure bias over much of the North Atlantic Ocean during the summer months (Fig. 3c), indicating a stronger NASH, which is consistent with the model's small AWP (Table 2). However, the ties between the AWP and the NASH are more complicated, as the atmosphere–ocean interactions affect each other. Grodsky et al. (2012) found that the CCSM4 exhibits a stronger climatological NASH and a stronger climatological polar low. Thus, the pressure gradient in the Atlantic increases, which is then associated with an increase in wind speed, an increase in latent heat loss, and cooler SSTs.

The differences in climatological ASO 925-hPa winds between R-2 and the five CMIP5 models in the TNA region are shown in Fig. 4. Immediately, it is evident that the increased easterly winds are most pronounced in the Caribbean region for the CCSM4, which is consistent with the model's small AWP bias. Similarly, the HadGEM2-ES, which has a more reasonable NASH, has stronger easterly winds in the Caribbean, possibly due to the southward bias in the position of the NASH (Fig. 4e). Stronger winds in the Caribbean and a weaker AWP in the HadGEM2-ES and

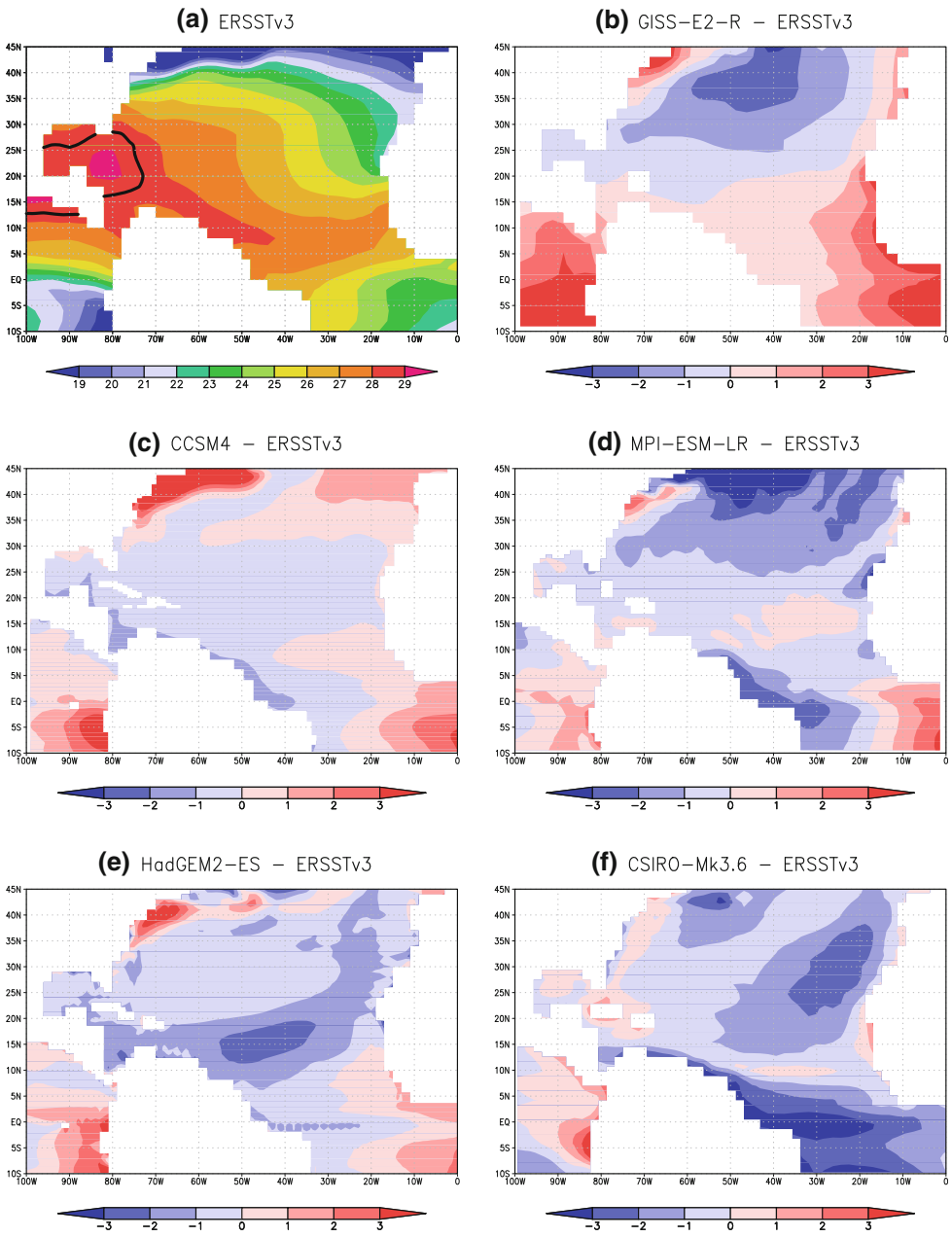


**Fig. 2** Differences in climatological 1909–2005 ASO averaged sea surface temperature (°C) in the Atlantic Basin between various models (**b**–**f**) and the ERSSTv3 is data plotted in (**a**). Once again the 28.5 °C isotherm is placed over the *shaded SSTs* in *panel* (**a**). The domain of these *plots* is from 0–45°N and 40–100°W

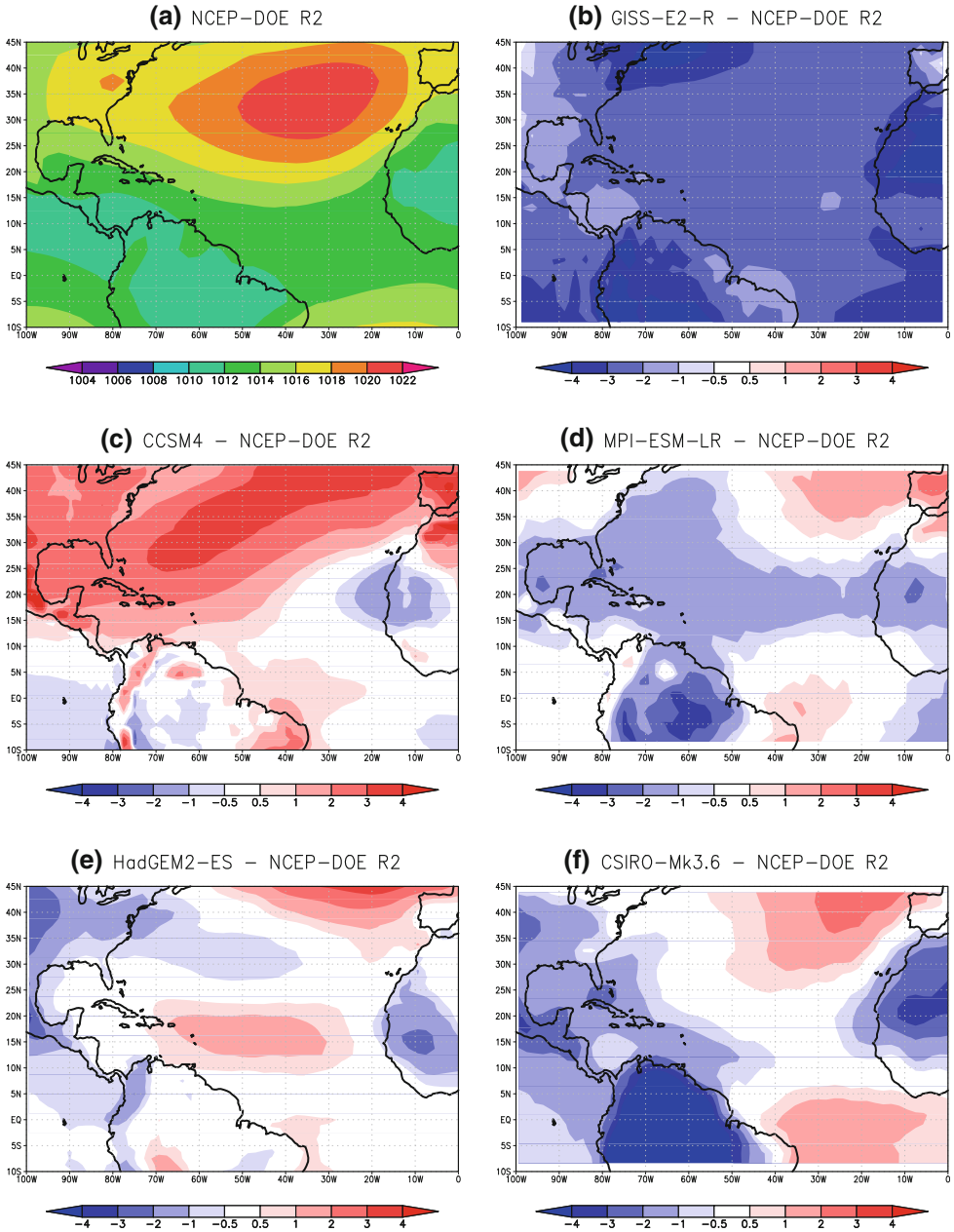


**Fig. 3** Differences in climatological 1909–2005 ASO averaged sea level pressure (hPa) in the Atlantic Basin between various models (**b**–**f**) and the NCEP-DOE Reanalysis *data plotted* in (**a**). The domain of these *plots* is from 0–45°N and 40–100°W

CCSM4 are consistent with the findings in past works that suggest the AWP is associated with a suppressed CLLJ in the region (Wang and Lee 2007). Ultimately, the complicated feedback between the NASH, the winds, and the AWP appears to be at the center of the cold SST bias in the IAS region for the CCSM4, HadGEM2-ES, and a number of the other CMIP5 models not specifically discussed in this section.

On the other hand, in the MPI-ESM-LR, it is evident that the strength of the 925-hPa easterly winds in the Caribbean, including the CLLJ, is diminished (Fig. 4b). The weaker winds in the IAS are consistent with the northeastward shift of NASH in the MPI-ESM-LR. Furthermore, the anomalously weaker winds in the MPI-ESM-LR are likely associated with its simulated AWP, which is larger than the AWPs in most other models. The more extreme pressure biases of NASH in the GISS-E2-R are associated with an even weaker pressure gradient force, and thus significantly weaker easterlies in the Caribbean (Fig. 4b). It is likely that because of these biases the GISS-E2-R is able to support the most realistically sized AWP.

### 3.3 Analysis of AWP variability in selected models

Building upon the discussions of AWP climatology in the CMIP5 models, this section focuses on analyzing the

variability of the AWPAI in the same five CMIP5 models emphasized in Sect. 3.2. Figure 5 shows the time series of the ASO AWPAI for each of the five models compared to the ERSSTv3 observations. In the most basic sense, the GISS-E2-R and MPI-ESM-LR appear to exhibit an appropriate magnitude of variability, compared to the SD of the AWPAI time series. The HadGEM2-ES, CSIRO-Mk3.6, and CCSM4, however, have an AWPAI SD less than half the magnitude of the observed AWPAI SD (Table 2), indicating that these models (as well as the majority of the other models) do not exhibit enough interannual and larger scale variability. Thus, the size of the AWP in each of these models incorrectly remains relatively consistent each year.

To highlight and evaluate the various modes of AWPAI variability within these five models with respect to the observations, spectral analyses are performed on these time series (Fig. 5) using a combination of the ensemble empirical mode decomposition (EEMD; Wu and Huang 2009) and the maximum entropy method (MEM; Ghil et al. 2002). The EEMD method is used to decompose the time series into a number of intrinsic mode functions (IMFs), which essentially decompose the total variability of the time series into distinct modes of temporal variability. For

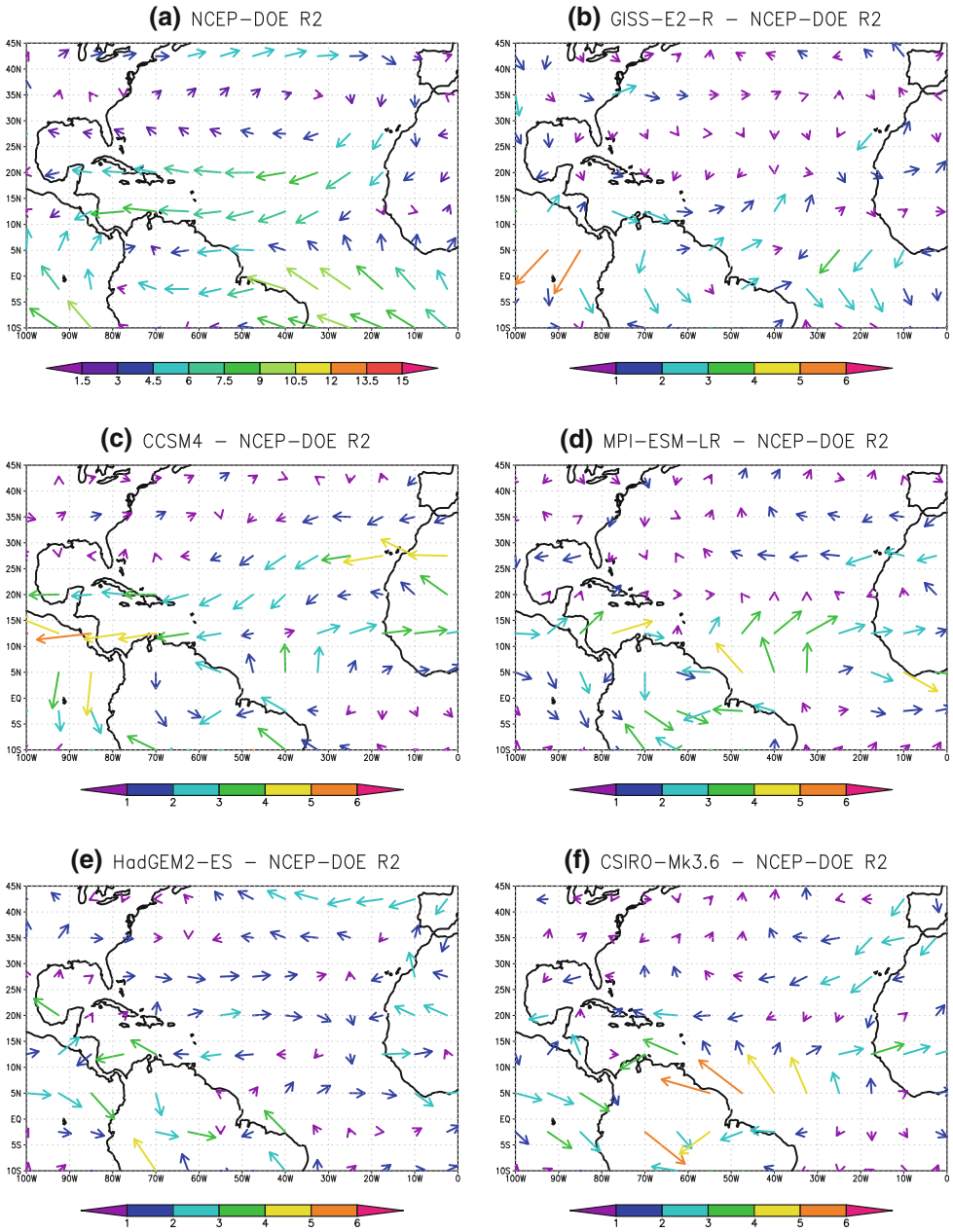


**Fig. 4** Differences in climatological 1909–2005 ASO averaged 925 hPa Winds in the Atlantic Basin between various models (**b**–**f**) and the NCEP-DOE Reanalysis *data plotted* in (**a**). The wind vectors are *color coded* by wind speeds (m/s). Note the difference in magnitudes between *panel* (**a**) and the other *five panels*. The domain of these plots is from 0–45°N and 40–100°W

the purpose of this study, the focus is on interannual scales of variability in the AWPAI, which is largely (but not entirely) accomplished by adding the first three IMFs and placing that sum through an MEM spectrum analysis using the Singular Spectrum Analysis–Multitaper Method Toolkit (SSA-MTM; Ghil et al. 2002). As will be shown in the ensuing discussion, the spectrum of AWP variations in the CMIP5 models show considerable disparity. Therefore, the first three IMFs in each of the models encompass a wide band of variations, making the low-pass filtering necessary to obtain a clearer picture of the low-frequency variations of the AWP. The resulting spectrum (Fig. 6) of this low-pass filtered dataset highlights the most dominant modes of variability from interannual time scales in the observations and the models.

The spectrum analysis of ERSSTv3-derived AWPAI has relative maxima occurring at periods of 2.6, 3.8, and 6.4 years (which easily passes the red noise test; not shown), suggesting that the AWPAI is influenced by oscillations of these periodicities. Furthermore, the periodicity of these modes of variability suggests that the AWP may share teleconnections with ENSO and the NAO, among other climate oscillations in the North Atlantic and global tropics. Such connections with ENSO and the NAO is supported by past works (e.g., Covey and Hastenrath 1978; Enfield and Mayer 1997; Czaja et al. 2002; Enfield et al. 2006; Liu et al. 2012) and are explored in greater detail later in this section.

In the spectral analysis, the CSIRO-Mk3.6 compares most favorably with respect to the observations, as it also has three spectral maxima with periods between 2.5 and 6.5 years. The correlation between the observed power spectrum and that of the CSIRO-Mk3.6 is highly significant at $r = 0.87$. The CCSM4's AWPAI power spectrum also is relatively similar to the observations with three maxima in the 2–10 year range and a correlation with the observed spectrum of $r = 0.63$. However, the power spectrums from the MPI-ESM-LR, HadGEM2-ES, and GISS-E2-R do not compare as favorably as those from the CSIRO-Mk3.6 or CCSM4. The GISS-E2-R is of particular concern, as it compares favorably to the rest of the models in terms of AWP size, but fails to replicate the observed modes of variability with a correlation near $r = 0$ and a maximum of spectral power at a longer period of 15.5 years.

Figure 7 shows correlations between the ASO-averaged AWPAI at zero-, one-, and two-season lags (AWP lagging) with global SSTs in the models and ERSSTv3 observations. Unsurprisingly, in the observations the AWPAI is most well correlated with SSTs in its residing IAS region. Correlations between the ASO AWPAI and IAS SSTs are highly significant at two- and one-season lags or the

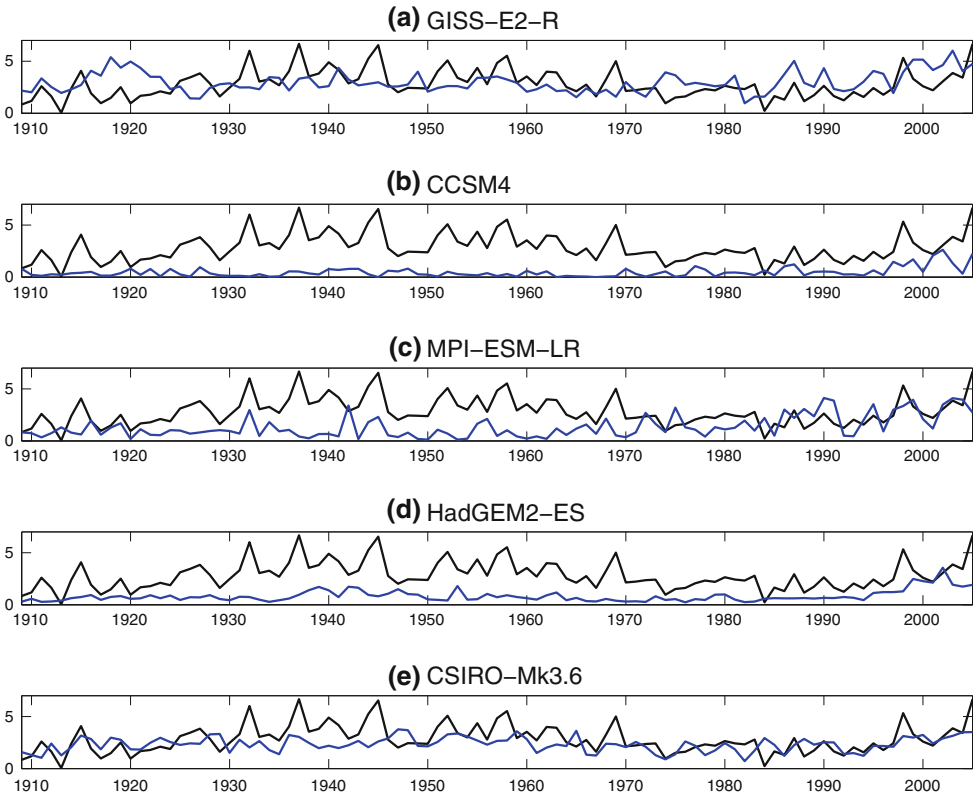


**Fig. 5** Annual time series measuring the ASO averaged AWPAI for ERSSTv3 (*black line* repeated in each *panel*) observations and various CMIP5 models (*blue line*). The index measures the areal coverage of the 28.5 °C SST isotherm in units of $10^6$ km. The area of this isotherm is calculated within the domain of 0–45°N; 40–100°W, excluding the waters of the eastern North Pacific in this region

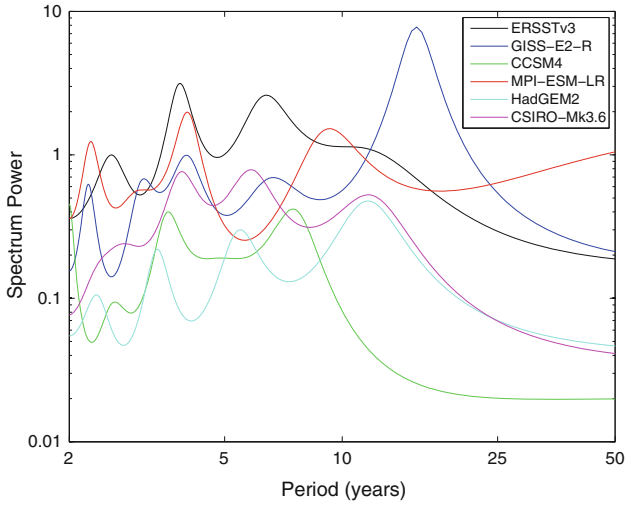


**Fig. 6** Maximum entropy spectrum (M = 10) of the 1909–2005 areal AWP index. To focus on variability from interannual-decadal time scales, the power spectrum is calculated for the sum of the first three IMFs of the AWP index, obtained through an ensemble empirical mode decomposition (EEMD)

preceding May–June–July (MJJ) and February–March–April (FMA) seasons, respectively, suggesting the importance of the intrinsic component of the AWP variations in the observations. More importantly the AWPAI in ASO is uncorrelated with the equatorial eastern Pacific SST variations at zero lag as pointed out in earlier studies (Lee et al. 2008; Misra et al. 2012).

However, Equatorial Eastern Pacific (EPAC) and equatorial Indian Ocean SST anomalies in preceding FMA and MJJ have a weak but statistically significant correlation with the ASO AWP variations, suggesting a potential, albeit weak, teleconnection to ENSO. However, any significant correlation between variations of the AWPAI and EPAC SSTs at zero lag (concurrent ASO) is limited to only the adjacent eastern North Pacific warm pool.

The ability to simulate the connections between AWPAI and Atlantic SSTs varies greatly from model to model. As expected, all five models have a high positive correlation ($r > 0.6$) between the ASO AWPAI and the collocated IAS SSTs at zero lag. However, the models poorly simulate the connections between the AWPAI and Atlantic SSTs at one- or two-season lags. The GISS-E2-R, CCSM4, HadGEM2-ES, and MPI-ESM-LR have significant correlations with preceding SSTs across the IAS as expected, but their magnitudes are under-represented, especially in the HadGEM2-ES. The CSIRO-Mk3.6 simulation is the most puzzling, as the AWPAI is more closely connected with preceding eastern Atlantic SSTs than it is with the collocated IAS SSTs.

Likewise, the models appear to have mixed results with regards to simulating ENSO's teleconnections with the AWP. The GISS-E2-R, the MPI-ESM-LR, and to a lesser extent the CSIRO-Mk3.6, tend to over-exaggerate ENSO's impact over the ASO AWP, especially at zero lag. The CCSM4 seems to handle the ENSO-AWP teleconnections most reasonably, with statistically significant correlations between variations of ENSO and the AWPAI at one- and two- season lags, and little to no correlation at zero-season lag. Unlike the other models, HadGEM2-ES has very little connection between the AWP and SSTs in the equatorial EPAC at two-, one-, and zero-season lags.

Table 5 contains correlations between the ASO AWPAI and various preceding and overlapping seasonal Niño3 measurements. These results further suggest that ENSO conditions in the spring and winter months have a significant relationship with the size of the summertime AWP later that year. The correlation between observed winter Niño3 and the following ASO AWPAI is significant to the 95 % CI. However, the correlations erode during the overlapping seasons, such that the correlation between June–August and September–November Niño3 SSTs and the ASO AWPAI are insignificant. Once again, with the exception of the HadGEM2-ES, the models exhibit too strong of an ENSO-AWP signal, which becomes statistically significant into the overlapping seasons for the GISS-E2-R and MPI-ESM-LR. A recently submitted paper noted that ENSO signals are much too strong in most of the CMIP5 models (Michael et al. 2012), which may help to explain their exaggerated influence over the AWP region.

Figure 8 shows the same correlations between global seasonal SSTs and the ASO AWPAI in the models and in the observations as Fig. 7, except at one- and two-season leads. The correlations between the AWPAI and TNA SSTs remain significant in the observations and reanalysis at one- and two-season leads, or the following November–December–January (NDJ) and FMA seasons, respectively, indicating that the AWP size affects the region's SSTs long after its demise in the late Northern Hemisphere autumn. However, it is evident that all five models underestimate the AWP's ability to influence succeeding TNA SSTs into the following winter, as the correlations are weak across the region at one- or two-season leads. The AWPAI has little significant correlation with the EPAC at one- or two-season leads in the observations and reanalysis, suggesting that the AWP has little bearing on the following winter's ENSO conditions in observations. This is supported by the correlations in Table 5, which indicate that the AWPAI is not significantly correlated to the late fall Niño 3 index in most cases. However, Fig. 8g, h reveal that the MPI-ESM-LR does have a significant positive correlation between the AWP and succeeding winter SSTs in the deep tropical Pacific Ocean.

The influence of the AWP's variations is not limited to SST responses, however. For example, Lee et al. (2008) showed that convection from variations in the AWP can

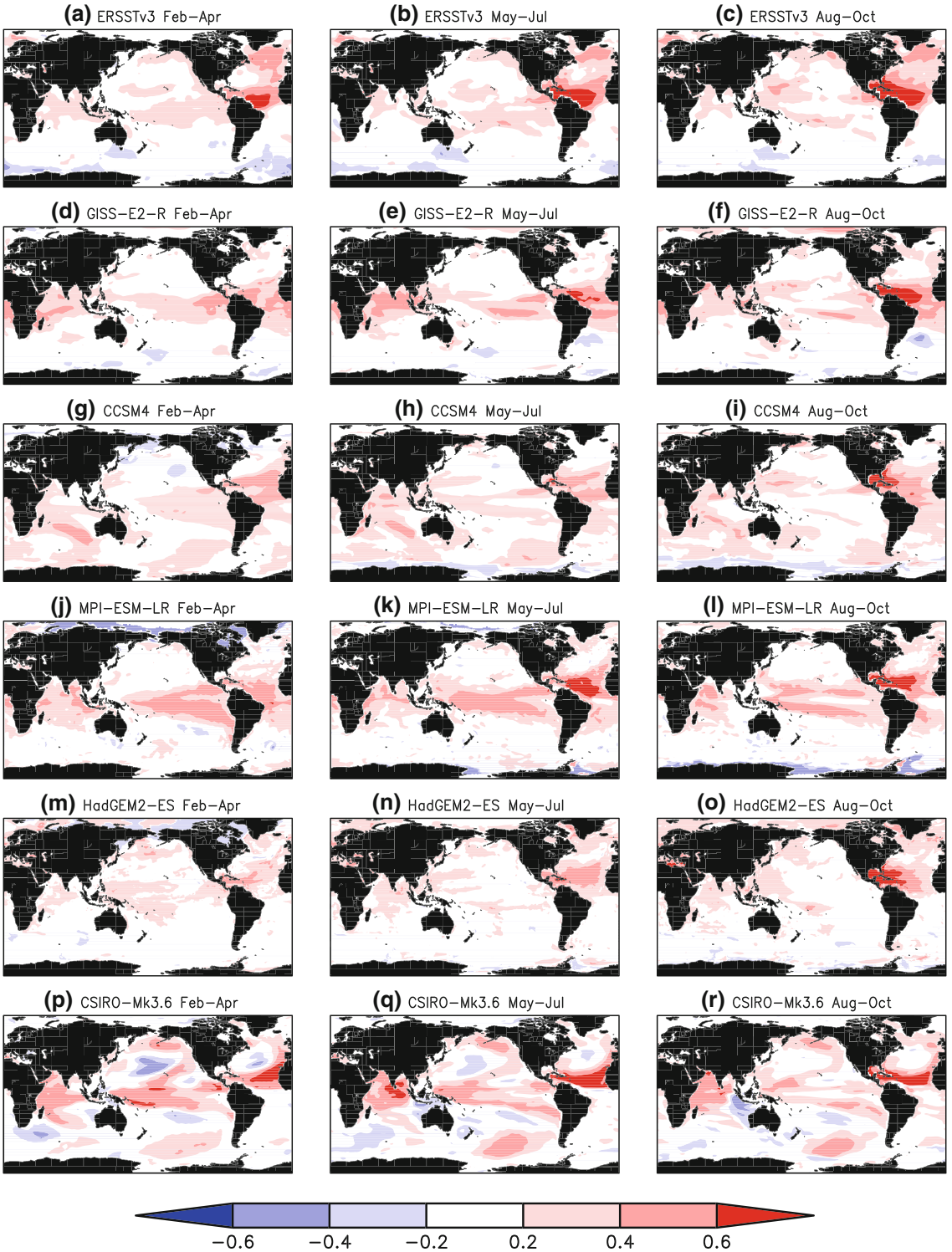


**Fig. 7** The correlation of 1909–2005 ASO averaged AWP area with (**a**) preceding February–March–April (FMA), (**b**) preceding May–June–July (MJJ), and (**c**) contemporaneous ASO global SSTA from ERSSTv3 observations. The remaining *panels* are similar to (**a**, **b** and **c**) but for five CMIP5 models (GISS-E2-R; CCSM4; MPI-ESM-LR; HadGEM2-ES; CSIRO-Mk3.6). Only statistically significant values at 95 % CI according to t test are shown

affect tropospheric temperatures by generating a Gill-type atmospheric response. This is similar to the well-known atmospheric warming response to warm ENSO events, in which the ENSO SST anomalies lead the tropospheric temperature anomalies by several months (Yulaeva et al. 1994; Chiang and Sobel 2002).

**Table 5** Correlations between 1910 and 2005 August–October averaged AWPAI and various preceding and concurrent seasonally averaged Nino3 measurements from the models and observations

| ASO AWPAI | Nino3 | | | |
|---|---|---|---|---|
| | DJF | MAM | JJA | SON |
| ERSSTv3 | *0.20* | *0.29* | 0.18 | 0.08 |
| GISS-E2-R | *0.36* | *0.44* | *0.22* | 0.19 |
| CCSM4 | *0.31* | *0.27* | 0.07 | 0.02 |
| MPI-ESM-LR | *0.45* | *0.48* | *0.29* | *0.24* |
| HadGEM2-ES | 0.18 | *0.26* | 0.07 | −0.06 |
| CSIRO-Mk3.6 | *0.48* | *0.36* | *0.25* | 0.15 |

Values highlighted in *italic font* are statistically significant at a 95 % CI

Figure 9 shows correlations between the ASO AWPAI and seasonal weighted tropospheric (250–850 hPa) temperature averages at one- and two-season leads (succeeding NDJ and FMA, respectively). In the observations, a significant correlation exists between variations of the ASO AWPAI and the succeeding averaged tropospheric temperatures in the global tropics, most notably over the Atlantic, Northern Africa, and Indonesia. The MPI-ESM-LR, GISS-E2-R, and CSIRO-Mk3.6 correlations are more significant and widespread than those seen in the observations. It is quite possible that these correlations are reflecting the well-known tendency for El Niño events to create warm atmospheric anomalies in the global tropics (Yulaeva et al. 1994), as these models over-exaggerate the correlations between ENSO and the AWP. This hypothesis is supported by the overly significant positive correlations between the summertime AWPAI and the preceding winter/spring Niño 3 indices in Table 5. If the warming of the tropical troposphere in the MPI-ESM-LR, GISS-E2-R, and CSIRO-Mk3.6 were a result of simply local TNA warming, the lag correlations in Table 5 would likely be insignificant. The CCSM4 appears to exhibit reasonable correlations between these temperatures and the AWPAI, whereas the HadGEM2-ES has weaker correlations throughout the globe at all leads.

## 4 Conclusions

Overall, we found that the CMIP5 models, as a whole, exhibit significant flaws in simulating the AWP climatology. Most of the 17 models analyzed in this study have a

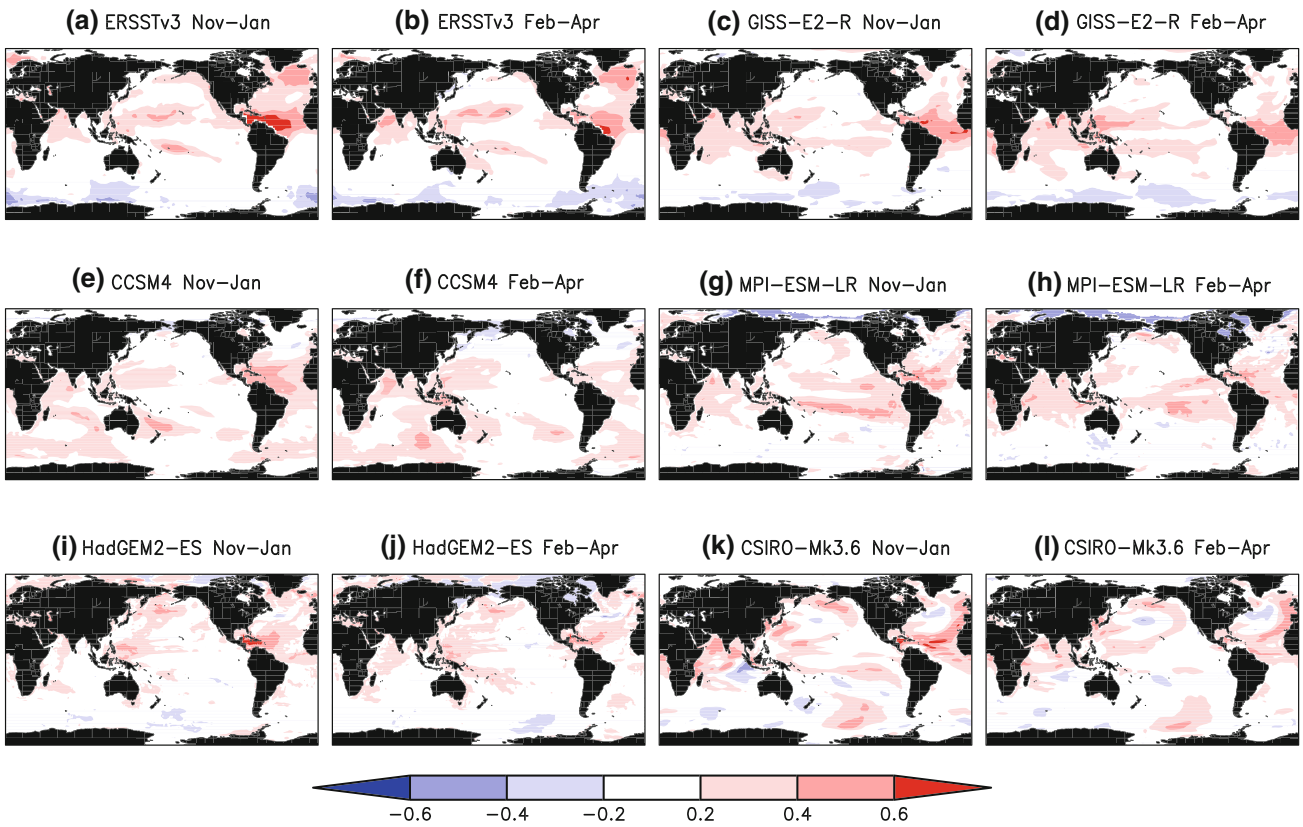


**Fig. 8** The correlation of 1909–2004 ASO averaged AWP area with (**a**) succeeding November–December–January (NDJ), (**b**) succeeding February–March–April (FMA) global SSTA from ERSSTv3 observations. The remaining *panels* are similar to (**a**) and (**b**) but for five CMIP5 models (GISS-E2-R; CCSM4; MPI-ESM-LR; HadGEM2-ES; CSIRO-Mk3.6). Only statistically significant values at 95 % CI according to t test are shown

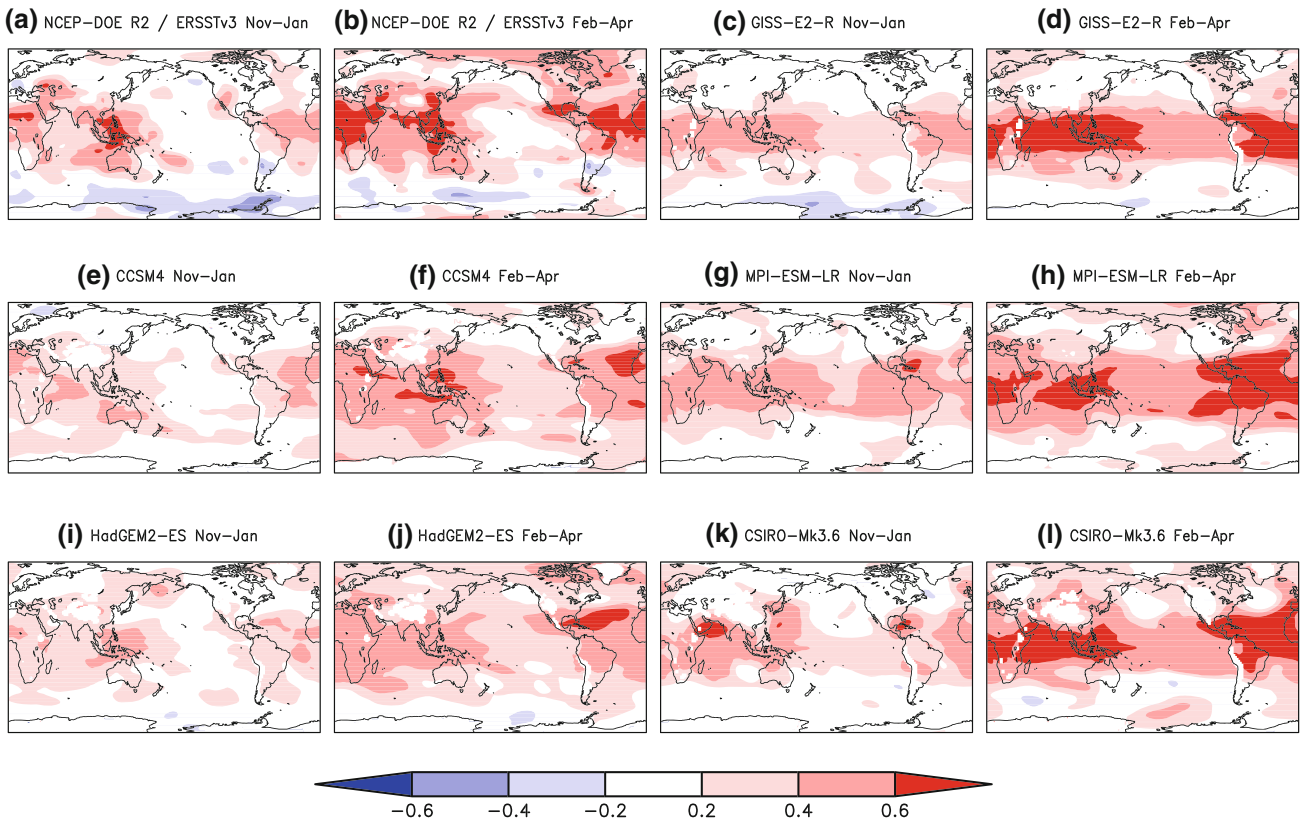


**Fig. 9** The correlation of 1979–2004 ASO averaged AWP area in ERSSTv3 observations with (**a**) succeeding November–December–January (NDJ), (**b**) succeeding February–March–April (FMA) global weighted troposphere air temperatures in NCEP-DOE Reanalysis 2. (**c–l**) from various CMIP5 models over the years 1909–2004. Only statistically significant values at 95 % CI according to t test are shown

significant cold SST bias in the TNA as a whole. The most successful models in terms of AWPAI climatology are the CSIRO-Mk3.6, MPI-ESM-LR, and the GISS-E2-R, as they have the most realistically sized AWP. These models also have the most realistic range of AWPAI values and reasonable seasonal cycles. However, they exhibit too broad of a seasonal peak of the AWP, and have deficiencies in representing the variability of the AWP.

More specifically, the GISS-E2-R produces the most reasonable climatological AWP size and location. The GISS-E2-R also compares most favorably to the observations in terms of its range and SD of ASO AWPAI values. Further examination shows flaws in the GISS-E2-R in way of its over exaggerated AWP-ENSO connections. In addition, the GISS-E2-R exhibits a noticeable low pressure bias especially over the continental regions surrounding the AWP. This raises the possibility that the GISS-E2-R is producing a reasonable solution largely because of the erroneous low pressure bias. The CSIRO-Mk3.6 similarly has a reasonably sized AWP and more encouragingly, it captures many of the observed modes of variability as discerned from spectral analysis. However, the AWP within the CSIRO-Mk3.6 is in an odd location, isolated over the Northern Caribbean because a cold bias exists over the Gulf of Mexico. Furthermore, it has an SST distribution that is too normally distributed. The CCSM4, on the other hand, does well in reproducing the various modes of variability, but it fails in producing an adequately sized AWP as a result of a significant cold bias. This same cold bias negatively affects the HadGEM2-ES simulation as well, as the model fails to reproduce the AWP's climatology, seasonal cycle, and other modes of variability. Finally, the MPI-ESM-LR has some success in terms of its ability to produce some observed aspects of the AWP's climatology, but its AWP appears to be driven too much by ENSO.

Ultimately, the model subsample discussed at length in Sect. 3 reveals that the CMIP5 models are not entirely successful in reproducing the observed climatology and variability of the AWP. Although strides have been made in improving the climate models with respect to the Pacific and particularly ENSO, the AWP and the TNA region as a whole is still misrepresented in many ways. The definition for the AWP used in observations highlights the problems associated with these CMIP5 models in the TNA region. The fact remains that all 17 of the CMIP5 models analyzed in this study underestimate the percentage of the North Atlantic basin that is covered by SSTs greater than 27 °C.

The pathological cold bias displayed by the majority of CIMP5 models relates to a more fundamental issue of temperatures not reaching a convective threshold needed to support organized large-scale convection in the Western Hemisphere. Although some models can capture the local SST variations and the secular rate of warming of SST despite the cold bias, these models will not represent the convective threshold, which is expected to increase in nature along with SST (Hoyos and Webster 2011). Moreover, by having a cold bias of about 1–2 °C, many of the models will misrepresent the local meridional overturning circulations and zonal transport of moisture. Thus, it is difficult to have confidence in the models' ability to simulate the AWP, and the TNA system as a whole, in a future climate.

Compared to previous models, most notably those included in CMIP3, the CMIP5 models contain many of the same biases relating to the AWP. For example, Liu et al. (2012) noted a similar strong cold bias in most of the CMIP3 models, which prevented many of the models from having an adequately sized AWP based on traditional definition. Furthermore, of the 22 CMIP3 models, only four were able to accurately depict the seasonal cycle, which as shown in Table 4, persisted to CMIP5. Like CMIP3, the models included in CMIP5 exhibited some connections to ENSO that are observed, but in most cases the relationships between ENSO and the AWP are too robust in CMIP5. As Liu et al. (2012) noticed with CMIP3, there appears to be at least one GCM in CMIP5 that can represent each aspect of climatology and variability well. However, no one model succeeds in representing all, or even most, of the characteristics of the observed AWP. Therefore, future work, especially studies focusing in greater detail on the causes of each of the noted Atlantic biases in the framework of the individual models, may yield significant improvement for interpreting the simulations from these and future climate models.

**Acknowledgments** We acknowledge the World Climate Research Programme's Working Group on Coupled Modelling, which is responsible for CMIP5, and thank the climate modeling groups listed in Table 1 for producing and making available their model output. We also thank the U.S. Department of Energy's Program for Climate Model Diagnosis and Intercomparison for providing coordinating support and leading development of software infrastructure in partnership with the Global Organization for Earth System Science Portals. Furthermore, we acknowledge that the Reanalysis 2 data were provided by NOAA/OAR/ESRL PSD, Boulder, Colorado, USA, from their Web site at http://www.esrl.noaa.gov/psd/. We are grateful for the thoughtful comments and suggestions provided by three anomous reviewers. Additionally, we thank Kathy Fearon for her helpful comments and revisions during the editing process. Finally, we thank Christopher Selman for helping to download the CMIP5 data, J-P Michael for helping to detrend the data, and Steven DiNapoli for providing the scripts used to calculate the AWPAI. This work was supported by grants from NOAA (NA12OAR4310078, NA10OAR4310215, NA11OAR4310110), USGS (06HQGR0125), and USDA (027865).

## References

Chang C-Y, Carton JA, Grodsky SA, Sumant N (2007) Seasonal climate of the tropical Atlantic sector in the NCAR Community Climate System Model 3: error structure and probable causes of errors. J Clim 20:1053–1070

Chang C-Y, Nigam S, Carton JA (2008) Origin of the springtime westerly bias in equitorial atlantic surface winds in the Community Atmosphere Model Version 3 (CAM3) simulation. J Clim 21:4766–4778

Chiang JCH, Sobel AH (2002) Tropical tropospheric temperature variations caused by ENSO and their influence on the remote tropical climate. J Clim 15:2616–2631

Clement Amy C, Seager R, Raghu M (2005) Why are there tropical warm pools? J Clim 18:5294–5311

Covey D, Hastenrath S (1978) The Pacific El Niño phenomenon and the Atlantic circulation. Mon Weather Rev 106:1280–1287

Czaja A, van der Vaart P, Marshall J (2002) A diagnostic study of the role of remote forcing in tropical Atlantic variability. J Clim 15:3280–3290

Davey M et al (2002) STOIC: a study of coupled model climatology and variability in tropical ocean regions. Clim Dyn 18:403–420

Enfield DB, Mayer DA (1997) Tropical Atlantic sea surface temperature variability and its relation to the El Niño Southern-Oscillation. J Geophys Res 102:929–945

Enfield DB, Lee S-K, Wang C (2006) How are large western hemisphere warm pools formed? Prog Oceanogr 70:346–365

Ghil M, Allen RM, Dettinger MD, Ide K, Kondrashov D, Mann ME, Robertson A, Saunders A, Tian Y, Varadi F, Yiou P (2002) Advanced spectral methods for climatic time series. Rev Geophys 40:3.1–3.41

Grodsky SA, Carton JA, Nigam S, Okumura YM (2012) Tropical Atlantic biases in CCSM4. J Clim 25:3684–3701. http://dx.doi.org/10.1175/JCLI-D-11-00315.1

Hoyos CD, Webster PJ (2011) Evolution of the tropical warm pool: past, present and future. Clim Dyn. doi:10.1007/s00382-011-1181-3

Kanamitsu M, Ebisuzaki W, Woollen J, Yang S-K, Hnilo JJ, Fiorino M, Potter GL (2002) NCEP-DOE AMIP-II reanalysis (R-2). Bull Am Meteorol Soc 83:1631–1643

Lee S-K, Enfield DB, Wang C (2007) What drives seasonal onset and decay of the Western Hemisphere warm pool? J Clim 20:2133–2146

Lee S-K, Enfield DB, Wang C (2008) Why do some El Niños have no impact on tropical North Atlantic SST? Geophys Res Lett 35:L16705

Liu H, Wang C, Lee S-K, Enfield D (2012) Atlantic warm pool variability in the IPCC-AR4 CGCM simulations. J Clim 25:5612–5628. http://dx.doi.org/10.1175/JCLI-D-11-00376.1

Michael JP, Misra V, Chassignet EP (2012) ENSO in historical simulations of CIMP5 models. Reg Environ Change (submitted)

Misra V, DiNapoli S (2012) The observed teleconnection between the equatorial Amazon and the Intra-Americas Seas. Clim Dyn. doi:10.1007/s00382-012-1474-1

Misra V, Chan S, Wu R, Chassignet E (2009) Air-sea interaction over the Atlantic warm pool in the NCEP CFS. Geophys Res Lett 36:L15702

Misra V, Stroman A, DiNapoli S (2012) The rendition of the Atlantic Warm Pool in the reanalyses. Clim Dyn. doi:10.1007/s00382-012-1503-0

Richter I, Xie S-P (2008) On the origin of equatorial Atlantic biases in coupled general circulation models. Clim Dyn 31:587–598

Richter I, Xie S-P, Wittenberg AT, Masumoto Y (2012) Tropical Atlantic biases and their relation to surface wind stress and terrestrial precipitation. Clim Dyn 38:985–1001

Rienecker MM et al (2011) MERRA: NASA's modern-era retrospective analysis for research and applications. J Clim 24: 3624–3648

Saha S et al (2010) The NCEP climate forecast system reanalysis. Bull Am Meteorol Soc 91:1015–1057

Smith TM, Reynolds RW, Peterson TC, Lawrimore J (2008) Improvements to NOAA's historical merged land-ocean surface temperature analysis (1880-2006). J Clim 21:2283–2296.

Taylor KE, Stouffer RJ, Meehl GA (2012) An overview of CMIP5 and the experiment design. Bull Am Meteorol Soc 93:485–498

Uppala SM et al (2005) The ERA-40 re-analysis. Q J R Meteorol Soc 131:2961–3012

Vizy EK, Cook KH (2010) Influence of the Amazon/Orinoco Plume on the summertime Atlantic climate. J Geophys Res 115:D21112

Wang C (2007) Variability of the Caribbean low-level jet and its relations to climate. Clim Dyn 29:411–422

Wang C, Enfield DB (2001) The tropical western hemisphere warm pool. Geophys Res Lett 28:1635–1638

Wang C, Enfield DB (2003) A further study of the tropical Western Hemisphere warm pool. J Clim 16:1476–1493

Wang C, Lee S (2007) Atlantic warm pool, Caribbean low-level jet, and their potential impact on Atlantic hurricanes. Geophys Res Lett 34:L02703

Wang C, Enfield DB, Lee S, Landsea CW (2006) Influences of the Atlantic warm pool on Western Hemisphere summer rainfall and Atlantic hurricanes. J Clim 19:3011–3028

Wang C, Lee S, Enfield DB (2007) Impact of the Atlantic warm pool on the summer climate of the Western Hemisphere. J Clim 20: 5021–5040

Wang C, Lee S, Enfield DB (2008) Atlantic warm pool acting as a link between Atlantic multidecadal oscillation and Atlantic tropical cyclone activity. Geochem Geophys Geosyst 9:Q05V03

Wang C, Lui H, Lee S, Atlas R (2011) Impact of the Atlantic warm pool on United States landfalling hurricanes. Geophys Res Lett 38:L19702

Wu Z, Huang NE (2009) Ensemble empirical mode decomposition: a noise-assisted data analysis method. Adv Adapt Data Anal 1:1–41

Yulaeva E, Holton JR, Wallace JM (1994) On the cause of annual cycle in the tropical lower stratopsheric temperature. J Atmos Sci 51:169–174